Available online at www.sciencedirect.com
ScienceDirect
Trans. Nonferrous Met. Soc. China 34(2024) 1204−1213
Transactions of Nonferrous Metals Society of China
www.tnmsc.cn

Synergistic strengthening and toughening of eutectic $C_xCoCr_3Fe_5Ni$ high entropy alloy

Si-rui HUANG, Ji-feng ZHANG, He-guo ZHU

College of Materials Science and Engineering, Nanjing University of Science and Technology, Nanjing 210094, China

Received 8 September 2022; accepted 11 April 2023

Abstract: $C_xCoCr_3Fe_5Ni$ (x=0, 0.1, 0.2 and 0.3, at.%) high entropy alloys (HEAs) were prepared via vacuum induction melting. The effects of carbon content on the microstructures and mechanical properties of the HEAs were intensively investigated. With the increase of the carbon content, the phase structure transforms from a dual-phase (FCC+BCC) to a eutectic mixture (FCC phase + $M_{23}C_6$ carbide). Compared to $CoCr_3Fe_5Ni$ base alloy, the $C_{0.2}CoCr_3Fe_5Ni$ eutectic HEA exhibits a significantly improved yield strength (from 307.5 to 378.9 MPa), ultimate tensile strength (from 646.5 to 837.1 MPa), and ductility (from 55.4% to 56.1%). It is shown that these comprehensive enhancements of strength and ductility result from the effect of interstitial solid solution strengthening by carbon alloying and second phase strengthening via the eutectic structure.

Key words: high entropy alloy; $M_{23}C_6$ carbide; eutectic structure; mechanical properties; strengthening mechanism

1 Introduction

Advanced alloys are the backbone of modern manufacturing engineering. Metallic alloys are typically used for manufacturing in structural applications that require high reliability, due to their excellent combination of strength and ductility. For decades, there has been an increasing demand of advanced alloys with a more superior combination of strength and ductility to meet the high-level requirements in aerospace/aircraft, defense, and automotive industry. Recently, excellent mechanical properties have been achieved [1−6] by high entropy alloys (HEAs), which comprise multiple principal elements with equiatomic or near equi-atomic concentrations at atomic scale. However, this kind of advanced alloys has not yet evaded the trade-off dilemma of strength−ductility [7−9]. For example, increasing Cr content can significantly enhance the mechanical strength of $Cr_xFeNiCu$ HEAs, but at the cost of their ductility [10]. Compared to TiNbZr, another example is $TiNbZrMo_{0.5}$ HEA. Its yield strength and compressive strength might be enhanced by 77.32% (up to 1.0 GPa) and 25.14% (up to 1.3 GPa), respectively; however, the compressive plasticity is decreased [11]. Therefore, it remains a challenge to enhance the strength of HEAs without compromising the ductility.

As for regulating the atomic ratios of these metallic elements, it was also reported that alloying with interstitial elements (e.g., B, C, and O elements) could be an efficient way to boost the mechanical properties of the transition metal-based HEAs [12−16]. It was found that the addition of interstitials into HEAs could result in much higher lattice distortions than substitutional elements which strongly influence the interaction with dislocations [17,18]. However, a few C-doped HEAs (CHEAs) have been developed and investigated, in order to break the strength−ductility

Corresponding author: He-guo ZHU, Tel: +86-13605182940, E-mail: zhg1200@njust.edu.cn
DOI: 10.1016/S1003-6326(24)66464-2

trade-off dilemma and achieve a superior combination of high strength and good plasticity. The experimental results showed that the addition of C element can not only produce significant surface hardening and synchronous toughening, but also result in prominent combination of strength and ductility [19−24]. For instance, with adding 2 at.% of interstitial C into the $Fe_{50}Mn_{30}Co_{10}Cr_{10}$ HEA, it was reported that the plastic strain of the matrix could be enhanced by 147.8%, without sacrificing its ultimate tensile strength (~550 MPa) [25].

As mentioned earlier, C element can be selected as the interstitial element based on the facts that C is one of the most widespread interstitials in alloys and the content is controllable during preparation of the alloys [17]. Inspired by those considerations, four kinds of $C_xCoCr_3Fe_5Ni$ (x=0, 0.1, 0.2 and 0.3) HEAs were prepared via vacuum induction melting in this study. To investigate the effect of C content on the microstructures and mechanical properties, microscopy and microanalysis were carried out with X-ray diffraction (XRD), scanning electron microscopy (SEM) and transmission electron microscopy (TEM).

2 Experimental

To fabricated samples of $C_xCoCr_3Fe_5Ni$ alloys, a few raw materials were used with high purity: cobalt particles (99.9%), chromium particles (99.99%), iron particles (99.99%), nickel particles (99.8%) and graphite powder (99.9%). Ingots were produced by vacuum induction melting under an argon atmosphere in a ceramic crucible. After the raw materials were melted and mixed completely, the molten metal liquid was then poured into a Cu mold and cooled down to room temperature in the furnace. The related details were described in our previous publication [26].

The microstructure and its composition were characterized by XRD (Bruker-AXS D8 Advance, and scanning rate of 5 (°)/min), SEM (Quant 250FEG) equipped with EDS (FEI Quanta 250 FEG), and TEM (FEI Talos F200X G2). I-shaped samples (2 mm in width, 1.1 mm in thickness, and 10.6 mm in length) were cut for tensile testing (UTM/CMT 5000, and the loading rate of 0.05 mm/min).

3 Results and discussion

3.1 Microstructure

The XRD patterns of $C_xCoCr_3Fe_5Ni$ HEAs are shown in Fig. 1. $CoCr_3Fe_5Ni$ primarily consists of the FCC phase with a small amount of the BCC phase. After adding 0.1 at.% of C element, the diffraction peak of the BCC phase disappears; that is, the phase composition changes from the FCC+BCC dual-phase structure to a single-phase FCC structure with the addition of C element. The disappearance of the BCC phase structure may be because C atoms tend to occupy the interstitial sites of the FCC lattice, improving the stability of the FCC phase [25,27,28]. When C content reaches 0.2 at.%, the diffraction peak intensity of the FCC (111) crystal plane decreases, while the diffraction peak intensity of the FCC (200) crystal plane increases, indicating that a strong texture of $[200]_{FCC}$ is formed in $C_{0.2}CoCr_3Fe_5Ni$. Carbides tend to form in $C_xCoCr_3Fe_5Ni$ alloys with higher C

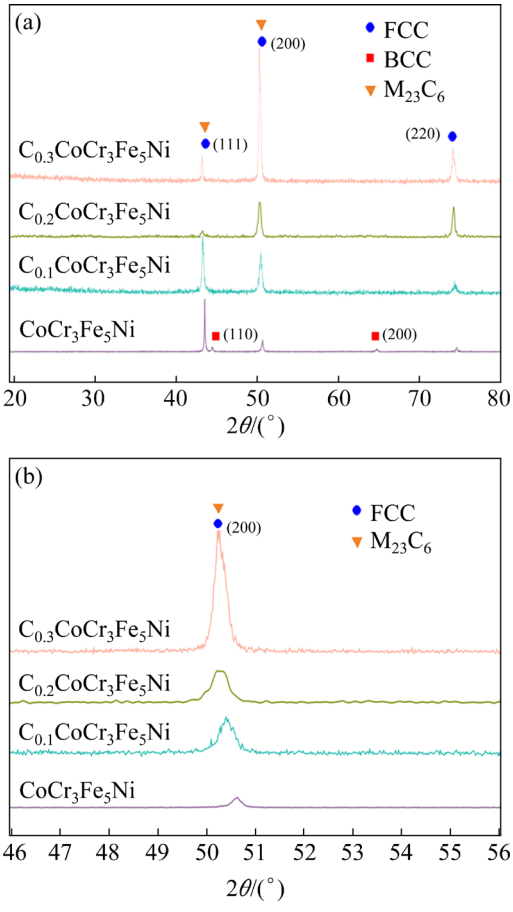

Fig. 1 XRD patterns of $C_xCoCr_3Fe_5Ni$ with different carbon contents (a) and enlarged XRD patterns with 2θ of 46°−56° (b)

contents because Fe and Cr have high affinity with element C, and thus, $M_{23}C_6$ carbides may be formed at grain boundaries in the alloys [29−33]. However, the diffraction peaks of the $M_{23}C_6$ compound are partially overlapped with those of the FCC phase. Therefore, the presence of $M_{23}C_6$ carbides may not be seen in the XRD patterns.

Figure 1(b) shows more details of the (200) peak of the FCC phase of the as-cast $C_xCoCr_3Fe_5Ni$ HEAs. It can be seen that the (200) peak shifts to lower 2θ values with increasing C content, which indicates an expansion of the FCC lattice parameter due to the dissolution of C into $C_xCoCr_3Fe_5Ni$ [29].

Figure 2 shows the microstructure of the as-cast $C_xCoCr_3Fe_5Ni$ HEA. As shown in Fig. 2(a), FCC equiaxed crystals and BCC cellular dendrite co-exist in the $CoCr_3Fe_5Ni$ HEA, in which the FCC phase is dominant. After adding 0.1 at.% C to the matrix (Fig. 2(b)), the microstructure of $C_{0.1}CoCr_3Fe_5Ni$ alloy consists of two parts, among which the gray structure (marked as Region A_2) is the matrix of the FCC phase. It is worth noting that the original dendrite structure is retained, and there is a tendency to form cellular crystals in some areas. The grain size does not change much, but thin strip-shaped white structure appears at the grain boundary. As shown in Fig. 3, the light lamellar structure (marked as Region C) located at the dendrite boundary is a typical eutectic structure. When the content of C element increases to 0.2 at.%, significant changes in the microstructure (Fig. 2(c)) can be observed compared to that of the base alloy; that is, the dendrite structure disappears and the matrix coalesces. According to the chemical compositions of different regions of $C_xCoCr_3Fe_5Ni$ alloys marked in Fig. 2 (Table 1), the regions labeled as A_{1-4} are the FCC phases enrich with elements Fe and Ni while the region labeled as B is the BCC phase enriched with element Cr, which have been confirmed in a previous work [26]. At the same time, C is detected in regions labeled as C_{2-4} of alloys, indicating that C has been solubilized into the matrix alloy. With increasing C content, the eutectic structure region of carbide (marked as Region C_3) and FCC phase (marked as Region A_3) increases. The eutectic structure still exists on the grain boundary of matrix grain, and the eutectic structure is parallel to the grain boundary of matrix. As shown in Fig. 2(d), when C content increases to 0.3 at.%, the eutectic structure looks similar to that in Fig. 2(b) but becomes more uniform, with the interface being more compact. However, there is no parallel growth relationship between eutectics and matrix.

As shown in Figs. 2(b−d), there is a layered microstructure in the area regarded as carbide. To further understand the layered structure, the $C_{0.2}CoCr_3Fe_5Ni$ HEA was analyzed by TEM. It can be seen from Fig. 4(a) that the $M_{23}C_6$ carbide is produced by crystallization in the matrix along the

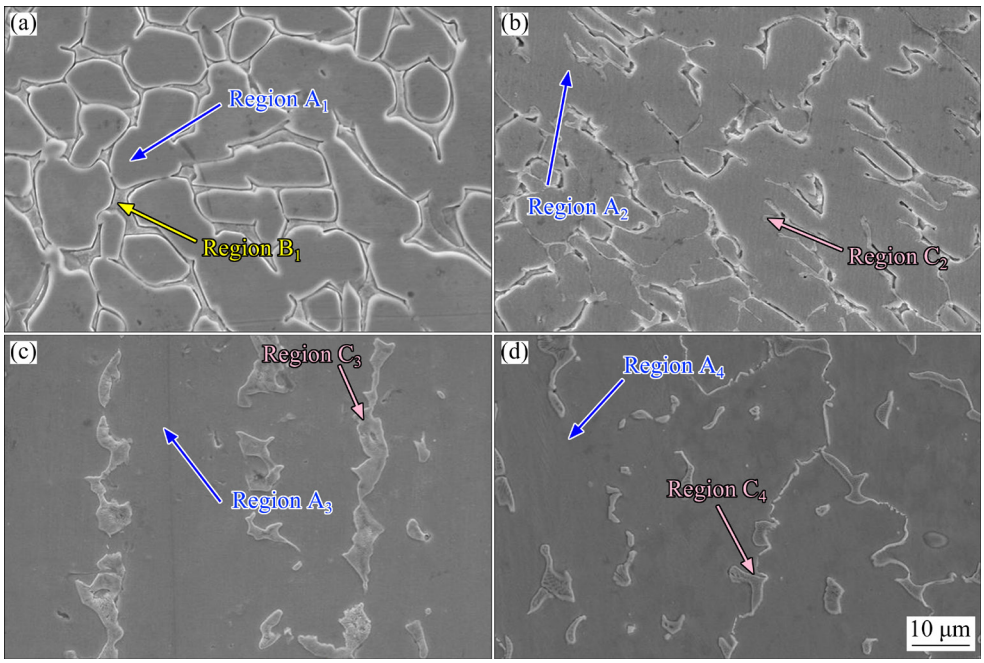

Fig. 2 SEM images of $C_xCoCr_3Fe_5Ni$ HEAs with different x values: (a) x=0; (b) x=0.1; (c) x=0.2; (d) x=0.3

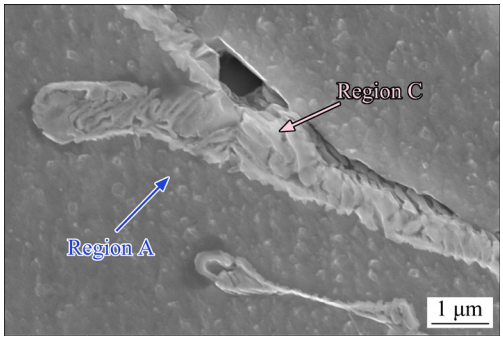

Fig. 3 SEM image of $C_{0.1}CoCr_3Fe_5Ni$ HEA

grain boundary, exhibiting a eutectic layered morphology within the FCC matrix. The average layer width of the carbide is about 95 nm. As shown in Fig. 4(b), according to the selected area electron diffraction pattern corresponding to Region A in Fig. 4(a), the carbide shows a $M_{23}C_6$ crystal structure. In previous research, $M_{23}C_6$ and M_7C_3 carbide particles were observed in carbon containing CoCrFeNiMn [34] and $Fe_{40.4}Ni_{11.3}Mn_{34.8}Al_{7.5}Cr_6$ HEA [35]. The other structure in the eutectic structure is proved to be FCC phase matrix (Fig. 4(c)). In addition, Fig. 4(d) shows the electron diffraction pattern of the selected region marked as "C" in Fig. 4(a) at the interface of the eutectic structure. The $M_{23}C_6$ with face centered cubic structure precipitated on the grain boundary has a complete coherent relationship with the matrix ($[001]_{FCC}$// $[001]_{M_{23}C_6}$, $(020)_{FCC}$//$(060)_{M_{23}C_6}$). The coherent interface causes a very low lattice mismatch, which can

Table 1 Chemical composition of various areas in $C_xCoCr_3Fe_5Ni$ HEAs marked in Fig. 2

Specimen	Region	Element content/at.%				
		Co	Cr	Fe	Ni	C
$CoCr_3Fe_5Ni$	A_1	9.6	27.3	52	11.1	0
	B_1	8.8	35.7	47.2	8.3	0
$C_{0.1}CoCr_3Fe_5Ni$	A_2	9.2	27.1	51.3	11	1.4
	C_2	7.4	28.3	33.7	7.1	23.5
$C_{0.2}CoCr_3Fe_5Ni$	A_3	8.9	26.9	50.5	10.6	3.1
	C_3	5.7	29.7	27.8	6.1	30.7
$C_{0.3}CoCr_3Fe_5Ni$	A_4	8.7	26.5	50.3	10.2	4.3
	C_4	4.1	33	22.5	3.6	36.8

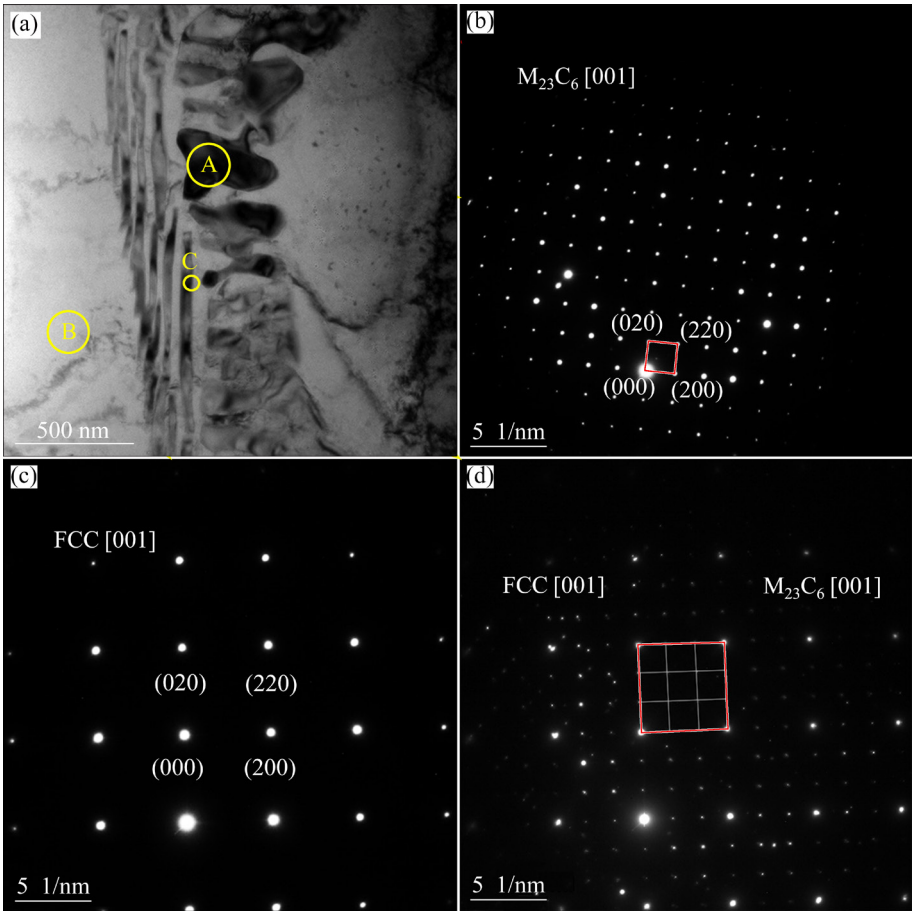

Fig. 4 TEM bright-field image of $C_{0.1}CoCr_3Fe_5Ni$ HEA (a); SAED patterns of $M_{23}C_6$ (b), FCC phase (c) and eutectic interface (d)

improve the elastic distortion near the precipitated phase and improve the uniform plastic deformation ability of the alloy [36]. The eutectic structure generally exists at the grain boundary because $M_{23}C_6$ carbides tend to be preferentially formed at the grain boundaries which are the preferred nucleation sites for heterogeneous nucleation [37−41].

The TEM and corresponding EDS mappings of the $C_{0.2}CoCr_3Fe_5Ni$ HEA are shown in Fig. 5. The layered eutectic structure shows clear interface with the matrix. The results of surface scanning indicate that the gray regions (marked as Region A) might be Cr-rich carbides. Combined with the analysis of XRD patterns above, the eutectic structure can be determined to be composed of $M_{23}C_6$ carbide and the FCC phase. It can be inferred that in the solidification process of the HEA, due to the redistribution of solute, the alloy shows a composition fluctuation at micron-scale. In this case, the redistribution of elements happens on the grain boundary; that is, Cr and C are enriched on the grain boundary. In this work, due to the increase of the proportion of Cr and Fe in the composition, $M_{23}C_6$ carbide can nucleate and grow on the grain boundary, so as to form eutectic structure with the matrix. In the $C_{0.2}CoCr_3Fe_5Ni$ alloy, the eutectic structure is parallel to the matrix. This is because in the solidification process, the faster cooling speed makes the plane solidification interface unstable. The small bulge of the solidification interface causes the enrichment of Cr, Fe and C solutes in the bulge groove to form complex carbides, which is inhibited by the growth direction of the matrix. Besides, the precipitated growth direction is roughly parallel to the growth direction of the matrix, which is similar to cellular crystal growth.

3.2 Mechanical properties

The Vickers hardness data of $C_xCoCr_3Fe_5Ni$ alloys obtained from Vickers hardness tests are shown in Table 2. The microhardness of the $C_{0.1}CoCr_3Fe_5Ni$ HEA reaches HV 309.9, which is 6.4% higher than that of $CoCr_3Fe_5Ni$ alloy. Pronounced increase of hardness is due to the formation of the hard $M_{23}C_6$ phase. On the other hand, the lattice distortion caused by interstitial solid solution strengthening of C increases the deformation resistance, thus increasing the hardness. However, the introduction of C element also results in the phase transformation from original BCC phase to the FCC phase, which reduces the hardness. Therefore, the increase in hardness of the $C_{0.1}CoCr_3Fe_5Ni$ alloy is not significant due to the combined effects of these two factors. With the further increase of C content to 0.2 and 0.3 at.%, the Vickers hardness increases to HV 342.4 and

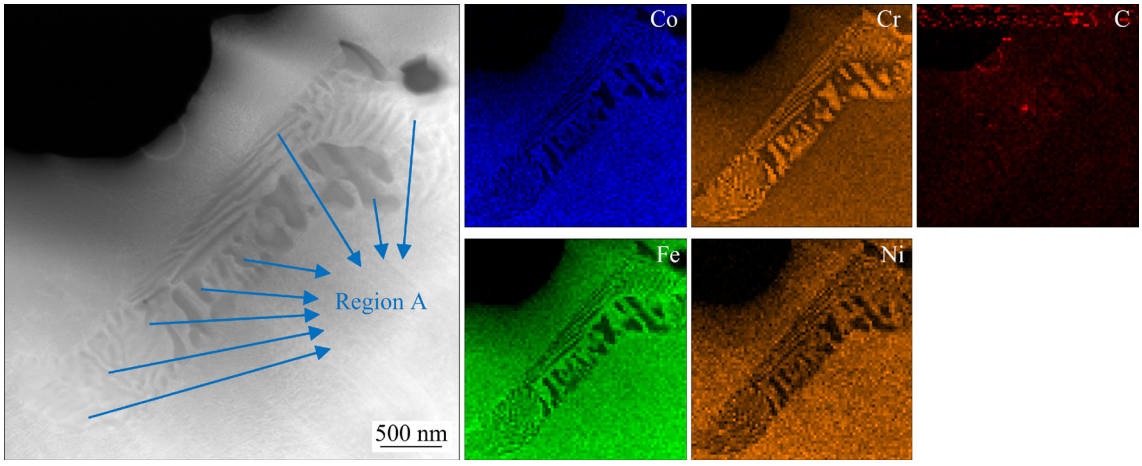

Fig. 5 TEM image and EDS elemental mappings of $C_{0.2}CoCr_3Fe_5Ni$ HEA

Table 2 Mechanical properties of $C_xCoCr_3Fe_5Ni$ HEAs

Alloy	Vickers hardness (HV)	Yield strength/MPa	Ultimate tensile strength/MPa	Elongation/%
$CoCr_3Fe_5Ni$	291.3	307.5	646.5	55.4
$C_{0.1}CoCr_3Fe_5Ni$	309.9	346.2	769.1	52.3
$C_{0.2}CoCr_3Fe_5Ni$	342.4	378.9	837.1	56.1
$C_{0.3}CoCr_3Fe_5Ni$	386.2	491.5	818.0	19.6

HV 386.2, respectively. Compared with the matrix, the hardness increases by 17.5% and 32.6%, respectively. This is because the C atom which enters the FCC lattice further improves the lattice distortion, as well as the increased content of hard $M_{23}C_6$ carbide [37], resulting in a significant improvement in microhardness.

Figure 6 exhibits tensile curves of as-cast $C_xCoCr_3Fe_5Ni$ HEAs. As given in Table 2, base alloy shows a relatively low yield strength (YS) of 307.5 MPa, ultimate tensile strength (UTS) of 646.5 MPa and uniform elongation of 55.4%. After the addition of 0.1 at.% C, the YS and UTS increase to 346.2 MPa and 769.1 MPa, respectively, while uniform elongation decreases to 52.3%. When the content of C increases to 0.2 at.%, the YS and UTS further increase to 378.9 MPa and 837.1 MPa, respectively, and more importantly, the uniform elongation increases to 56.1%. This means both strength and ductility are enhanced simultaneously. Generally, the addition of C improves the yield strength of FCC-structured HEAs, but at the expense of ductility [34]. Surprisingly, by comparing the tensile properties of $C_{0.2}CoCr_3Fe_5Ni$ and $CoCr_3Fe_5Ni$, it is found that the addition of C improves not only the YS (increased by 23.2%), but also the UTS and elongation, increased by 29.5% and 1.3% respectively. However, when C content is further increased to 0.3 at.%, the YS and UST are about 491.5 MPa and 818.0 MPa, respectively, with the elongation decreasing to 19.6%.

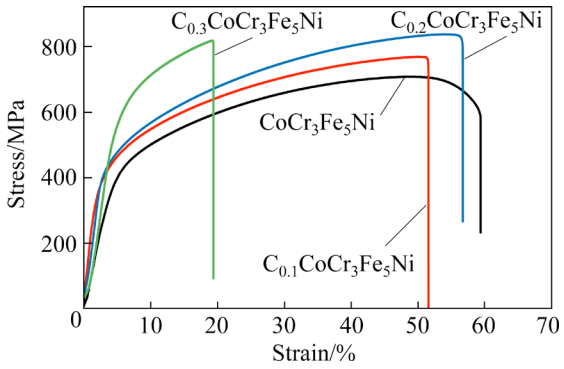

Fig. 6 Tensile curves of $C_xCoCr_3Fe_5Ni$ HEAs at room temperature

Figure 7 shows the fracture morphologies of $C_xCoCr_3Fe_5Ni$ (x=0, 0.1, 0.2 and 0.3) HEAs. As shown in Fig. 7(a), dense dimples distribute on the fracture surface of $CoCr_3Fe_5Ni$, which indicates a ductile fracture mode. Compared with the microstructure shown in Fig. 2(a), the grain boundary of cellular dendrite is relatively flat, which is conducive to crack propagation. Therefore, during tensile fracture, the crack propagates along the grain boundary of cellular dendrite, and the flat grain boundary leads to the generation of a large number of tearing edges. The crack then coalesces in the dendrite region of the cellular dendrite, and finally leads to the fracture of the material. When x=0.1, as shown in Fig. 7(b), a small amount of C addition changes fracture morphology significantly. A layered fracture is formed on a part of the macro fracture

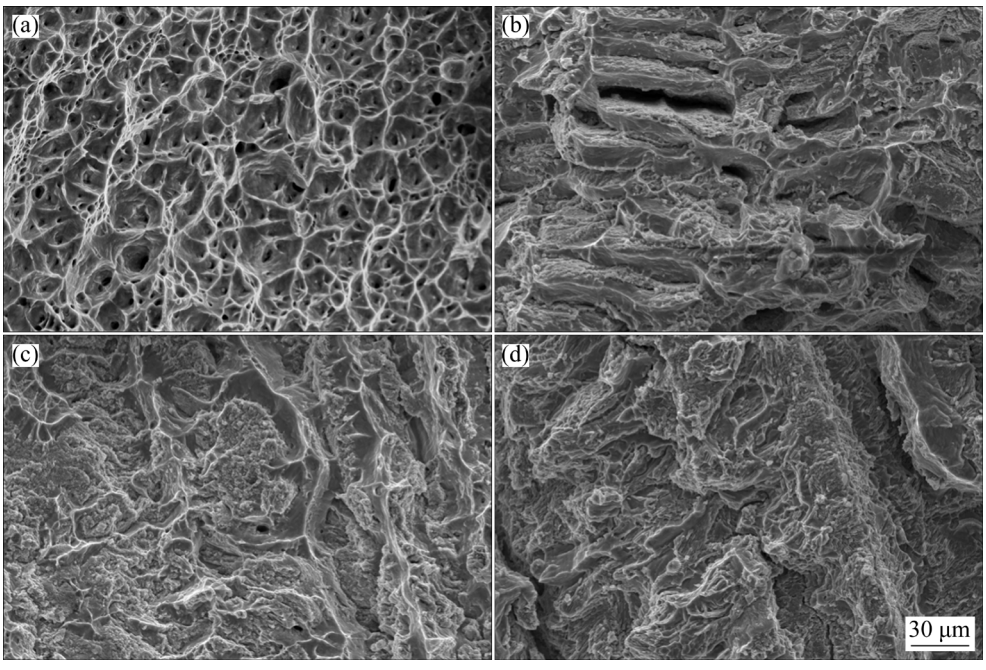

Fig. 7 Fracture morphologies of $C_xCoCr_3Fe_5Ni$ HEAs with different x values: (a) x=0; (b) x=0.1; (c) x=0.2; (d) x=0.3

surface, and there is an obvious boundary between layers. Corresponding to the cellular structure in Fig. 2(b) and the fine strip eutectic structure at the grain boundary, it can be seen that the crack first occurs at the grain boundary during tensile fracture, and then the crack propagates along the grain boundary. Because of the coherent interface between the eutectic structure and the matrix, the strength of grain boundaries is high, so, some cracks begin to expand from the inside of the grain to form a river pattern. When x=0.2 (Fig. 7(c)), the fracture morphology is also composed of two parts. One part of the morphology is similar to honeycomb, which means intense plastic flow and a large number of dimples. It belongs to ductile fracture, which corresponds to the FCC phase grains in microstructure. Outside the honeycomb dimple, there are obvious tear ridges and dissociation surfaces, which correspond to the eutectic structure at the grain boundary. Similar to the microstructure, the tear ridge on the fracture surface also has an obvious direction, indicating that due to the existence of eutectic structure completely coherent with the matrix, the grain and grain boundary bear the load at the same time, and the strength is the same. The fracture type belongs to the mixed ductile and brittle fracture. When x=0.3, there is no dimple, and the laminar flow pattern still exists, showing quasi cleavage fracture (Fig. 7(d)).

3.3 Strengthening mechanism

Compared with the $CoCr_3Fe_5Ni$ alloy, the YS, UTS and elongation of the $C_{0.2}CoCr_3Fe_5Ni$ alloy are increased by 23.2%, 29.5% and 1.3%, respectively. The improvement of the tensile properties of the $C_{0.2}CoCr_3Fe_5Ni$ alloy is caused by a synergistic effect of solid solution strengthening, grain boundary strengthening, dislocation strengthening and stacking fault energy (SFE). Firstly, solution strengthening is mainly due to different atomic sizes. Solute atom C exists in the interstitial sites of the FCC phase in the $CoCr_3Fe_5Ni$ HEA, which greatly increases lattice distortion, produces stress field and increases the resistance of dislocation movement, so as to achieve the effect of strengthening. Solution strengthening mainly comes from the elastic interaction (size effect) and modulus interaction between dislocation and solute atoms.

In addition, the introduction of C allows the phase transformation from BCC to FCC in the matrix, resulting in the increased plasticity. Moreover, the eutectic structure consisting of the FCC phase matrix and $M_{23}C_6$ carbide formed at grain boundaries greatly hinders the grain boundary movement and improves the strength of the alloy due to grain boundary strengthening [17,29,42,43]. Besides, as a hard phase, $M_{23}C_6$ carbide acts as an obstacle to dislocation movement. In the process of dislocation movement, the dislocations entangle with each other. These dislocations overlap and crisscross to form a high-density dislocation wall, which hinders the movement of dislocations and makes plastic deformation difficult, so as to improve the strength [44]. As discussed above, $M_{23}C_6$ and the matrix have a coherent relationship, which reduces the mismatch and elastic distortion near the $M_{23}C_6$ carbide, effectively mitigates the microscopic elastic distortion around the precipitated phase particles and improves the macroscopic homogeneous plastic deformation capacity of the alloy, resulting in the improved plasticity [34,36,41].

Moreover, as an inherent property of materials, SFE has an important influence on the deformation mechanism of FCC metals. In the case of medium to high-level fault energy, lateral slip becomes prevalent. With the decrease of SFE, cross slip becomes more difficult and deformation twins are activated [45,46]. Previous research on high entropy alloys shows that SFE is significantly dependent on C concentration [31]. Besides, PETROV's research reveals that the SFE of Fe−C FCC alloys will decrease first and then increase with higher C content [47]. It was found that the increase in the SFE may lead to a transition from phase change induced plasticity (TRIP) to twinning induced plasticity (TWIP), thus improving the plasticity of the alloy [25]. Therefore, with the addition of C content in as-cast $CoCr_3Fe_5Ni$ high entropy alloy, the change of plasticity may be attributed to that of SFE; that is, the plasticity increases first and then decreases again.

4 Conclusions

(1) With the addition of carbon element to the $CoCr_3Fe_5Ni$ matrix (base alloy), the crystal structure transforms from an FCC+BCC dual-phase

structure into a single FCC structure. Moreover, the eutectic structure is introduced into the grain interior, which is composed of $M_{23}C_6$ carbide and FCC matrix. The $M_{23}C_6$ carbide shows coherent orientation relationship with the FCC matrix, which has the interphase orientation relationships of $[001]_{FCC}//[001]_{M_{23}C_6}$, and $(020)_{FCC}//(060)_{M_{23}C_6}$.

(2) The Vickers hardness, YS and UTS of the optimal $C_{0.2}CoCr_3Fe_5Ni$ are increased to HV 342.4, 378.9 MPa and 837.1 MPa, respectively. It is also noted that the elongation is also increased by 1.3%, from 55.4% (matrix) to 56.1%, which shows that the approach in this study can significantly enhance the strength without sacrificing its elongation.

(3) The carbon element acts as the interstitial solution atom in the base alloy, strengthening the grain boundaries of the $CoCr_3Fe_5Ni$ HEAs. Furthermore, the eutectic structure effectively restricts the dislocation motion, which could contribute to the strengthening and toughening in the $CoCr_3Fe_5Ni$ HEAs simultaneously.

CRediT authorship contribution statement

Si-rui HUANG: Methodology, Formal analysis, Data curation, Writing − Original draft; **Ji-feng ZHANG:** Conceptualization, Supervision, Methodology; **He-guo ZHU:** Funding acquisition, Writing – Review & editing, Methodology.

Declaration of competing interest

The authors declare that they have no known competing financial interests or personal relationships that could have appeared to influence the work reported in this paper.

Acknowledgments

This work was supported by the National Natural Science Foundation of China (No. 51571118).

References

[1] TIAN Yu-sheng, ZHOU Wen-zhe, TAN Qing-biao, WU Ming-xu, QIAO Shen, ZHU Guo-liang, DONG An-ping, SHU Da, SUN Bao-de. A review of refractory high-entropy alloys [J]. Transactions of Nonferrous Metals Society of China, 2022, 32: 3487−3515. https://doi.org/10.1016/S1003-6326(22)66035-7.

[2] HE Zhu-feng, JIA Nan, WANG Hong-wei, LIU Yu-jie, LI Dong-yue, SHEN Yong-feng. The effect of strain rate on mechanical properties and microstructure of a metastable FeMnCoCr high entropy alloy [J]. Materials Science and Engineering A, 2020, 776: 138982. https://doi.org/10.1016/j.msea.2020.138982.

[3] YAN Xue, XU Jian-yan, GUAN Xiang-he, HAN Bing-yuan, ZHANG Cheng, CUI Zi-ruo, LIANG Wen-ping. Optimization of microstructure and properties of laser sintered $Ni_{30}Cr_{25}Al_{15}Co_{15}Mo_5Ti_5Y_5$ high-entropy alloy coatings via controlling plasma [J]. Transactions of Nonferrous Metals Society of China, 2023, 33: 168−188. https://doi.org/10.1016/S1003-6326(22)66098-9.

[4] XU Qin, CHEN De-zhi, WANG Cong-rui, CAO Wen-chao, WANG Qi, CUI Hong-zhi, ZHANG Shu-yan, CHEN Rui-run. Effects of La on microstructure and mechanical properties of $NbMoTiVSi_{0.2}$ refractory high entropy alloys [J]. Transactions of Nonferrous Metals Society of China, 2021, 31: 512−520. https://doi.org/10.1016/S1003-6326(21)65513-9.

[5] SHABANI A, TOROGHINEJAD M R. Evaluation of microstructure and texture formation during annealing of cold-rolled FeCrCuMnNi multiphase high-entropy alloy [J]. Transactions of Nonferrous Metals Society of China, 2020, 30: 449−462. https://doi.org/10.1016/S1003-6326(20)65225-6.

[6] XU Jun, CAO Cheng-ming, GU Ping, PENG Liang-ming. Microstructures, tensile properties and serrated flow of Al CrMnFeCoNi high entropy alloys [J]. Transactions of Nonferrous Metals Society of China, 2020, 30: 746−755. https://doi.org/10.1016/S1003-6326(20)65250-5.

[7] CHEN Liang-bin, WEI Ran, TANG Ke, ZHANG Jin-yu, JIANG Feng, HE Lin, SUN Jun. Heavy carbon alloyed FCC-structured high entropy alloy with excellent combination of strength and ductility [J]. Materials Science and Engineering A, 2018, 716: 150−156. https://doi.org/10.1016/j.msea.2018.01.045.

[8] QIN Gang, XUE Wen-tian, CHEN Rui-run, ZHENG Hui-ting, WANG Liang, SU Yan-qing, DING Hong-sheng, GUO Jing-jie, FU Heng-zhi. Grain refinement and FCC phase formation in AlCoCrFeNi high entropy alloys by the addition of carbon [J]. Materialia, 2019, 6: 100259. https://doi.org/10.1016/j.mtla.2019.100259.

[9] LI Zhi-ming, PRADEEP K G, DENG Yun, RAABE D, TASAN C C. Metastable high-entropy dual-phase alloys overcome the strength-ductility trade-off [J]. Nature, 2016, 534: 227−230. https://doi.org/10.1038/nature17981.

[10] WU Hao, HUANG Si-rui, ZHU Cheng-yan, ZHU He-guo, Xie Zong-han. Influence of Cr content on the microstructure and mechanical properties of $Cr_xFeNiCu$ high entropy alloys [J]. Progress in Natural Science: Materials International, 2020, 30: 239−245. https://doi.org/10.1016/j.pnsc.2020.01.012.

[11] CHEN Geng-biao, YAN Hong-wei, WANG Zhe, WANG Kai-ming, YVES N I, TONG Yong-gang. Effects of Mo content on the microstructure and mechanical properties of $TiNbZrMo_x$ high-entropy alloys [J]. Journal of Alloys and Compounds, 2023, 930: 167373. https://doi.org/10.1016/j.jallcom.2022.167373.

[12] FENG Jun-jie, GAO Shuo, HAN Kun, MIAO Yi-dong, QI Ji-qiu, WEI Fu-xiang, REN Yao-jian, ZHAN Zhen-zhen, SUI Yan-wei, SUN Zhi, CAO Peng. Effects of minor B addition on microstructure and properties of $Al_{19}Co_{20}Fe_{20}Ni_{41}$ eutectic high-entropy alloy [J]. Transactions of Nonferrous Metals

Society of China, 2021, 31: 1049−1058. https://doi.org/10.1016/S1003-6326(21)65560-7.

[13] KO Jun Yeong, hong Sun Ig. Microstructural evolution and mechanical performance of carbon-containing CoCrFeMnNi-C high entropy alloys [J]. Journal of Alloys and Compounds, 2018, 743: 115−125. https://doi.org/10.1016/j.jallcom.2018.01.348.

[14] CHEN Yi-wen, LI Yun-kai, CHENG Xing-wang, XU Zi-qi, WU Chao, CHENG Bo, WANG Meng. Interstitial strengthening of refractory $ZrTiHfNb_{0.5}Ta_{0.5}O_x$ (x=0.05, 0.1, 0.2) high-entropy alloys [J]. Materials Letters, 2018, 228: 145−147. https://doi.org/10.1016/j.matlet.2018.05.123.

[15] SEOL J B, BAE J W, LI Zhi-ming, HAN J C, KIM J G, RAABE D, KIM H S. Boron doped ultrastrong and ductile high-entropy alloys [J]. Acta Materialia, 2018, 151: 366−376. https://doi.org/10.1016/j.actamat.2018.04.004.

[16] YE You-xiong, OUYANG Bin, LIU Chain-tsuan, DUSCHER Gerd-j, NIEH Tai-gang. Effect of interstitial oxygen and nitrogen on incipient plasticity of NbTiZrHf high-entropy alloys [J]. Acta Materialia, 2020, 199: 413−424. https://doi.org/10.1016/j.actamat.2020.08.065.

[17] LI Zhi-ming. Interstitial equiatomic CoCrFeMnNi high-entropy alloys: Carbon content, microstructure, and compositional homogeneity effects on deformation behavior [J]. Acta Materialia, 2019, 164: 400−412. https://doi.org/10.1016/j.actamat.2018.10.050.

[18] TSIANIKAS S J, CHEN Yu-jie, JJEONG J, ZHANG Si-yuan, XIE Zong-han. Forging strength-ductility unity in a high entropy steel [J]. Journal of Materials Science & Technology, 2022, 113: 158−165. https://doi.org/10.1016/j.jmst.2021.10.019.

[19] CHUNG K S, LUAN J H, SHEK Chan-hung. Strengthening and deformation mechanism of interstitially N and C doped FeCrCoNi high entropy alloy [J]. Journal of Alloys and Compounds, 2022, 904: 164118. https://doi.org/10.1016/j.jallcom.2022.164118.

[20] SHEN Shang-kun, CHEN Fei-da, TANG Xiao-bin, LIN Ji-wei, GE Guo-jia, LIU Jian. Effects of carbon doping on irradiation resistance of $Fe_{38}Mn_{40}Ni_{11}Al_4Cr_7$ high entropy alloys [J]. Journal of Nuclear Materials, 2020, 540: 152380. https://doi.org/10.1016/j.jnucmat.2020.152380.

[21] XIN Ben-bin, ZHANG Ai-jun, HAN Jie-sheng, SU Bo, MENG Jun-hu. Tuning composition and microstructure by doping Ti and C for enhancing mechanical property and wear resistance of $Al_{0.2}Co_{1.5}CrFeNi_{1.5}Ti_{0.5}$ high entropy alloy matrix composites [J]. Journal of Alloys and Compounds, 2020, 836: 155273. https://doi.org/10.1016/j.jallcom.2020.155273.

[22] LU Er-yang, MAKKONEN I , MIZOHATA K, LI Zhi-ming. Effect of interstitial carbon on the evolution of early-stage irradiation damage in equi-atomic FeMnNiCoCr high-entropy alloys [J]. Journal of Applied Physics, 2020, 127: 025103. https://doi.org/10.1063/1.5130748.

[23] LU Er-yang, ZHAO Jun-lei, MAKKONEN I, MIZOHATA K, LI Zhi-ming, HUA Meng-yuan, DJURABEKOVA F, TUOMISTO F. Enhancement of vacancy diffusion by C and N interstitials in the equiatomic FeMnNiCoCr high entropy alloy [J]. Acta Materialia, 2021, 215: 117093. https://doi.org/10.1016/j.actamat.2021.117093.

[24] FU Zheng-hong, WU Peng-fei, ZHU Shu-ya, GAN Ke-fu, YAN Ding-shun, LI Zhi-ming. Effects of interstitial C and N on hydrogen embrittlement behavior of non-equiatomic metastable FeMnCoCr high-entropy alloys [J]. Corrosion Science, 2022, 194: 109933. https://doi.org/10.1016/j.corsci.2021.109933.

[25] LIU Xiu-lan, ZHAO Xue-rou, CHEN Jian, LÜ Yu-kun, WANG Xian-hui, LIU Bin, LIU Yong. Effect of C addition on microstructure and mechanical properties of as-cast HEAs $(Fe_{50}Mn_{30}Co_{10}Cr_{10})_{100-x}C_x$ [J]. Materials Chemistry and Physics, 2020, 254: 123501. https://doi.org/10.1016/j.matchemphys.2020.123501.

[26] ZHANG Ji-feng, QIU Huan, ZHU He-guo, XIE Zong-han. Effect of Al additions on the microstructures and tensile properties of $Al_xCoCr_3Fe_5Ni$ high entropy alloys [J]. Materials Characterization, 2021, 175: 111091. https://doi.org/10.1016/j.matchar.2021.111091.

[27] HE Meng-yuan, SHEN Yong-feng, JIA Nan, LIAW P K. C and N doping in high-entropy alloys: A pathway to achieve desired strength-ductility synergy [J]. Applied Materials Today, 2021, 25: 101162. https://doi.org/10.1016/j.apmt.2021.101162.

[28] FAN Jian-tao, ZHANG Li-jun, YU Peng-fei, ZHANG Meng-di, LIU Da-jin, ZHOU Zheng, CUI Peng, MA Ming-zhen, JING Qin, LI Gong, LIU Ri-ping. Improved the microstructure and mechanical properties of AlFeCoNi high-entropy alloy by carbon addition [J]. Materials Science and Engineering A, 2018, 728: 30−39. https://doi.org/10.1016/j.msea.2018.05.013.

[29] MORAVCIK I, HORNIK V, MINARIK P, LI Lin-lin, DLOUHY I, JANOVSKA M, RAABE D, LI Zhi-ming. Interstitial doping enhances the strength-ductility synergy in a CoCrNi medium entropy alloy [J]. Materials Science and Engineering A, 2020, 781: 139242. https://doi.org/10.1016/j.msea.2020.139242.

[30] GUO Lin, OU Xiao-qin, NI *S*ong, LIU Yong, SONG Min. Effects of carbon on the microstructures and mechanical properties of FeCoCrNiMn high entropy alloys [J]. Materials Science and Engineering A, 2019, 746: 356−362. https://doi.org/10.1016/j.msea.2019.01.050.

[31] CHEN Li, LI Zhan-jiang, DAI Pin-qiang, FU Pei-xin, CHEN Jun-feng, TANG Qun-hua. Effects of carbon addition on microstructure and mechanical properties of $Fe_{50}Mn_{30}Co_{10}Cr_{10}$ high-entropy alloy prepared by powder metallurgy [J]. Journal of Materials Research and Technology, 2022, 20: 73−87. https://doi.org/10.1016/j.jmrt.2022.07.067.

[32] PENG Jian, LI Zi-yong, JI Xin-bo, SUN Yan-le, FU Li-ming, SHAN Ai-dang. Decomposition kinetics of carbon-doped FeCoCrNiMn high-entropy alloy at intermediate temperature [J]. Transactions of Nonferrous Metals Society of China, 2020, 30: 1884−1894. https://doi.org/10.1016/S1003-6326(20)65347-X.

[33] QIN Gang, XUE Wen-tian, FAN Cheng-lei, Chen Rui-run, WANG Liang, Su Yan-qing, DING Hong-sheng, GUO Jing-jie. Effect of Co content on phase formation and mechanical properties of $(AlCoCrFeNi)_{100-x}Co_x$ high-entropy alloys [J]. Materials Science and Engineering A, 2018, 710: 200−205. https://doi.org/10.1016/j.msea.2017.10.088.

[34] ZHOU Y J, ZHANG Y, WANG Y L, CHEN G L. Solid solution alloys of AlCoCrFeNiTi$_x$ with excellent room-temperature mechanical properties [J]. Applied Physics Letters, 2007, 90: 181904. https://doi.org/10.1063/1.2734517.

[35] CHEN Jian, CHEN Zhi-hao, WANG Xiao-bo, LU Yu-kun, WANG Xian-hui, LIU Yong, FAN Xin-hui. Effect of C content on microstructure and tensile properties of as-cast CoCrFeMnNi high entropy alloy [J]. Materials Chemistry and Physics, 2018, 210: 136−145. https://doi.org/10.1016/j.matchemphys.2017.08.011.

[36] HIRTH J, COHEN M. On the strength-differential phenomenon in hardened steel [J]. Metallurgical Transactions, 1970, 1: 3−8. https://doi.org/10.1007/BF028 19235.

[37] STEPANOV N, YURCHENKO N Y, TIKHONOVSKY M A, SALISHCHEV G A. Effect of carbon content and annealing on structure and hardness of the CoCrFeNiMn-based high entropy alloys [J]. Journal of Alloys and Compounds, 2016, 687: 59−71. https://doi.org/10.1016/j.jallcom.2016.06.103.

[38] WANG Zhang-wei, BAKER Ian, GUO Wei, POPLAWSKY J D. The effect of carbon on the microstructures, mechanical properties, and deformation mechanisms of thermo-mechanically treated $Fe_{40.4}Ni_{11.3}Mn_{34.8}Al_{7.5}Cr_6$ high entropy alloy [J]. Acta Materialia, 2017, 126: 346−360. https://doi.org/10.1016/j.actamat.2016.12.074.

[39] JIANG Sui-he, WANG Hui, WU Yuan, LIU Xiong-jun, CHEN Hong-hong, YAO Meng-ji, GAULT B, PONGE D, RAABE D, HIRATA A, CHEN Ming-wei, WANG Yan-dong, LU Zhao-ping. Ultrastrong steel via minimal lattice misfit and high-density nanoprecipitation [J]. Nature, 2017, 544: 460−464. https://doi.org/10.1038/nature22032.

[40] ASTAFUROVA E, MELNIKOV E, ASTAFUROV S, REUNOVA K, PANCHENKO M, MOSKVINA V, TUMBUSOVA I. A comparative study of a solid solution hardening in carbon-alloyed FeMnCrNi$Co_{0.95}C_{0.05}$ high-entropy alloy subjected to different thermal-mechanical treatments [J]. Materials Letters, 2021, 285: 129073. https://doi.org/10.1016/j.matlet.2020.129073.

[41] WU Wei-feng, GAO Niu, LIU Xin-wang, GUO Wen-tao, YANG Li, FAN Zi-tian. Precipitation behavior of carbides in a low-carbon NiCoFeCr high-entropy alloy at 800 °C [J]. Materials Letters, 2021, 298: 130020. https://doi.org/10.1016/j.matlet.2021.130020.

[42] Jägle Eric A, MITTEMEIJER E J. The kinetics of grain-boundary nucleated phase transformations: Simulations and modelling [J]. Acta Materialia, 2011, 59: 5775−5786. https://doi.org/10.1016/j.actamat.2011.05.054.

[43] PENG Jian, LI Zi-yong, Fu Li-ming, JI Xin-bo, PANG Zhuo-rui, SHAN Ai-dang. Carbide precipitation strengthening in fine-grained carbon-doped FeCoCrNiMn high entropy alloy [J]. Journal of Alloys and Compounds, 2019, 803: 491−498. https://doi.org/10.1016/j.jallcom.2019.06.204.

[44] CHEN Yu-jie, AN Xiang-hai, ZHANG Sam, FANG Feng, HUO Wen-yi, MUNROE Paul, XIE Zong-han. Mechanical size effect of eutectic high entropy alloy: Effect of lamellar orientation [J]. Journal of Materials Science & Technology, 2021, 82: 10−20. https://doi.org/10.1016/j.jmst.2020.11.067.

[45] MA Xiao-Guang, CHEN Jian, CHEN Zheng, YAN Wen. Evolution of microstructure and texture of cold-drawn polycrystalline Ag with low stacking fault energy [J]. Science Chian Technological Sciences, 2015, 58: 1146−1153. https://doi.org/10.1007/s11431-015-5862-8.

[46] CHEN Yu-jie, CHEN Deng-ke, AN Xiang-hai, ZHANG Yin, ZHOU Zhi-feng, LU Song, MUNROE P, ZHANG S, LIAO Xiao-zhou, ZHU Ting, XIE Zong-han. Unraveling dual phase transformations in a CrCoNi medium-entropy alloy [J]. Acta Materialia, 2021, 215: 117112. https://doi.org/10.1016/j.actamat.2021.117112.

[47] PETROV Y N. On the carbon distribution at structural imperfections in manganese austenite [J]. Scripta Metallurgica et Materialia, 1993, 29: 1471−1476. https://doi.org/10.1016/0956-716X(93)90339-T.

共晶高熵合金 $C_xCoCr_3Fe_5Ni$ 强度−韧性协同效应

黄思睿，张继峰，朱和国

南京理工大学 材料科学与工程学院，南京 210094

摘　要：通过真空感应熔炼制备 $C_xCoCr_3Fe_5Ni$ (x=0, 0.1, 0.2 和 0.3，摩尔分数)高熵合金(HEAs)，研究碳含量对微观结构和力学性能的影响。随着碳含量的增加，合金相结构由 FCC+BCC 双相结构转变为 $M_{23}C_6$ 碳化物和 FCC 相的共晶结构。与 $CoCr_3Fe_5Ni$ 基体合金(屈服强度 307.5 MPa、极限抗拉强度 646.5 MPa 以及伸长率 55.4%)相比，$C_{0.2}CoCr_3Fe_5Ni$ 共晶 HEA 的屈服强度(378.9 MPa)、极限抗拉强度(837.1 MPa)和伸长率(56.1%)均显著提高。该合金力学性能的提高主要归因于碳合金化所引起的间隙固溶强化和特殊的共晶结构带来的第二相强化。

关键词：高熵合金；$M_{23}C_6$ 碳化物；共晶组织；力学性能；强化机制

(Edited by Bing YANG)